THE ASTROPHYSICAL JOURNAL, 289:220–237, 1985 February 1

CHEMISTRY IN DYNAMICALLY EVOLVING CLOUDS

SHANKAR P. TARAFDAR,[1] SHEO S. PRASAD, AND WESLEY T. HUNTRESS, JR.
Jet Propulsion Laboratory, California Institute of Technology

KAREN R. VILLERE
Board of Studies in Astronomy and Astrophysics, University of California, Santa Cruz

AND

DAVID C. BLACK
Space Science Division, NASA/Ames Research Center
Received 1983 August 3; accepted 1984 July 17

ABSTRACT

We present a unified model of chemical and dynamical evolution of isolated, initially diffuse and quiescent interstellar clouds. This model uses a semiempirically derived dependence of the observed cloud temperatures on the visual extinction and density. Even low-mass, low-density, diffuse clouds can collapse in this model, because the inward pressure gradient force assists gravitational contraction. In contrast, previous isothermal collapse models required the low-mass diffuse clouds to be unrealistically cold before gravitational contraction could start. Theoretically predicted dependences of the column densities of various atoms and molecules, such as C and CO, on visual extinction in diffuse clouds are in accord with observations. Similarly, our predicted dependences of the fractional abundances of various chemical species (e.g., CO, H_2CO, CN, HCN, HCO^+) on the total hydrogen density in the core of the dense clouds also agree with observations reported to date in the literature. Compared with previous models of interstellar chemistry, the present model has the potential to explain the wide spectrum of chemical and physical properties of both diffuse and dense clouds with a common formalism employing only a few simple initial conditions.

Subject headings: interstellar: molecules — molecular processes

I. INTRODUCTION

This paper has been motivated by two important issues. The first concerns the possible existence of a unifying link underlying the great diversity exhibited by interstellar clouds. On one end of the spectrum are the very diffuse clouds ($n \sim 10$–100 cm^{-3}, $60 \leq T \leq$ a few hundred Kelvin, and visual extinction $A_v < 1$), where the matter is mostly in atomic form and even simple diatomic species such as CO, OH are barely visible. On the other end of the spectrum we have dense clouds ($n \sim 10^5$–10^6 cm^{-3}) which are very cool ($T \sim 10$–20 K) and dark ($A_v > 8$). In sharp contrast with the situation in diffuse clouds, chemical processing in dark clouds is quite advanced, so that matter is predominantly in molecular form and complex polyatomic molecules (e.g., methanol, ethanol, ketene) are widespread. We have attempted to identify a common thread among this diversity through the underlying process of hydrodynamical-chemical evolution. Our theme is that a gravitationally unstable mass of gas may manifest the various diffuse and dense cloud properties at one time or another, depending upon the stage of its evolution. Thus we may think of families of interstellar clouds. A given family would consist of both diffuse and dense clouds but would differ from other families with respect to only simple initial conditions. The fact that clouds may evolve from low- to high-density states under the influence of gravitational collapse has been anticipated for quite some time (see, e.g., reviews by Woolfson 1979; Larson 1973; McNally 1971; Bodenheimer 1968; Taylor 1968; Hayashi 1966). However, as noted by Woolfson (1979) these studies of gravitational collapse were concerned with clouds that were already dense and not far from a protostellar stage. Successful attempts to model collapse of low-mass, low-density diffuse clouds into dense clouds were limited to clouds with very low temperatures of the order of 10 K (see, e.g., Villere and Black 1980 and references therein). Unfortunately, real diffuse clouds do not have such low temperatures. Collapse of warm diffuse clouds therefore was thought to need assistance from either external triggers (such as compression by shocks) or thermal-chemical instabilities (Oppenheimer and Dalgarno 1975; Glassgold and Langer 1976; Sabano and Kannari 1978; Kannari, Sabano, and Tosa 1979). It is therefore interesting that the present study has been able to investigate the collapse of realistically warm diffuse clouds of mass as low as 40 $M_\odot$ and initial density as low as 140 cm^{-3} without needing any assistance from instabilities or triggers. We start with quite diffuse ($A_v \leq 0.5$) states of these clouds and are able to model their collapse to central densities of the order of 10^6 cm^{-3} and visual extinction $A_v \gtrsim 100$. Furthermore, we have studied the evolution of many observable properties such as column abundances and local abundances of various chemical species. By comparing our theoretical results with observation, we also show the possibility that hydrodynamical evolution may indeed provide a unifying link in the apparent extreme diversity of interstellar clouds. Previously, Gerola and Glassgold (1978), Suzuki *et al.* (1976), and Kiguchi *et al.* (1974) reported calculations of chemistry in a gravitationally collapsing cloud. Models of Kiguchi *et al.* (1974) and Suzuki *et al.* (1976) are of limited validity because they consider clouds in free fall. Gerola and Glassgold (1978) reported a much more detailed and meaningful calculation. The distinction between Gerola and

[1] NASA–NRC Senior Resident Research Associate, 1981–1983, on leave from Tata Institute of Fundamental Research, Bombay, India.

Glassgold's (1978) study and the present study is that the former limited their calculation to just one massive cloud ($M = 2.5 \times 10^4\ M_\odot$ and $A_v \approx 2$), which was already quite advanced in its journey from a diffuse to a dense state. Also, they neither posed nor dwelt upon the fundamental issue that motivated us.

The second motivation for the present modeling of the chemistry of dynamically evolving clouds is to address some purely chemical issues. Most previous studies of interstellar chemistry (Graedel, Langer, and Frerking 1982; Prasad and Huntress 1980*a*, *b*, hereafter PH; Mitchell, Ginsburg, and Kuntz 1978; Black and Dalgarno 1977; Pickles and Williams 1977; Glassgold and Langer 1974; Herbst and Klemperer 1973; Solomon and Klemperer 1972; Iglesias 1977; de Jong, Dalgarno, and Boland 1980) are equilibrium models. These models have been very useful by providing a good understanding of interstellar chemistry. Nevertheless, several problem areas remain which call for evolutionary models. For example, the relative abundance of cyanopolyynes and chemically related C_3N is higher in TMC-1 than in L183, which has quite similar physical properties. This may possibly be due to non–steady state conditions in a dynamically evolving cloud (see also Irvine *et al.* 1981). Furthermore, all clouds may not be in equilibrium. For example, observations of internal velocity dispersions of the order of 0.5–1 km s^{-1} also suggest that many of the dark clouds around the Milky Way are probably collapsing (Larson 1973). More recently, Lequeux (1977) has presented additional evidence for collapsing clouds, and, indeed, Villere and Black (1980, 1982) find that certain observed properties of several dark clouds are consistent with their being in a state of collapse. Thus, models of chemistry in dynamically collapsing clouds are clearly needed. The present study attempts to meet this need, albeit in a limited way in the beginning, while addressing the fundamental issues posed earlier.

II. THE THEORETICAL MODELS: HYDRODYNAMICS AND CHEMISTRY

We start with spherically symmetrical, homogeneous, and quiescent clouds of gas of various masses, and, as a simplifying assumption, neglect rotation, turbulence and magnetic fields. Justifications for this simplification can be found in the references cited earlier (e.g., Gerola and Glassgold 1978). The gravitational collapse of such a gas cloud is governed by the following Lagrangian equations of motion:

$$\frac{1}{\rho}\frac{\partial P}{\partial r} + \frac{Gm}{r^2} + \frac{\partial^2 r}{\partial t^2} = 0 \tag{1}$$

and

$$1 - 4\pi r^2 \rho \frac{\partial r}{\partial m} = 0\ , \tag{2}$$

which are solved subject to the boundary condition of specified constant pressure at the cloud surface (see, e.g., Bodenheimer 1968). The independent variables are the mass m interior to a spherical interface, and the time t. Radius r, mass density ρ, and pressure P are dependent variables, and $G = 6.67 \times 10^{-8}$ cgs units is the gravitational constant. Hydrodynamics and chemistry are coupled because the gas pressure P is related to the mean molecular mass μ and the temperature T:

$$P = RT/\mu\ , \tag{3}$$

where

$$1/\mu = \Sigma_i(\chi_i/m_i)\ , \tag{4}$$

$$T = f(\rho, A_v, \chi_{C^+}, \chi_C, \chi_{CO}, \ldots)\ , \tag{5}$$

and χ_i and m_i are the mass fraction and the mass of the ith species and A_v is the visual extinction. Fractional abundances of C^+, C, and CO enter into equation (5) because these are the major coolants. Visual extinction A_v affects the temperature of the cloud because both the photoelectric heating rate and the fractional abundances of the coolants are dependent on A_v. Chemistry influences hydrodynamics through equation (4) because $H \rightarrow H_2$ conversion affects μ, the mean molecular mass, and through equation (5) because $C^+ \rightarrow C \rightarrow CO$ conversion by chemical processing affects the temperature structure.

The temperature structure of a cloud is of paramount importance in its collapse. Consider for illustration a cloud of uniform initial density. Use of a grossly approximate form of equation (5), such as the polytropic T-ρ relation, leads to conditions where the pressure gradient force is vanishingly small initially. Thus, the widely used isothermal approximation causes serious problems for collapsing low-mass homogeneous clouds. In fact, it is not possible to evolve a low-mass dense cloud ($m \leq 100\ M_\odot$) from a diffuse cloud state under the isothermal condition if realistic diffuse cloud temperatures ($T \sim 60$–80 K) are used in the initial condition. This led many investigators to use unrealistically low ($T \sim 10$ K) temperatures even in the initial diffuse stage (see Villere and Black 1980 and references therein). In contrast, according to equation (5) the temperature in the assumed cloud would decrease toward the center because A_v increases toward the center, which causes a decrease in the photoelectron heating and an increase in molecular cooling by CO (see, e.g., expressions for photoelectic heating and the behavior of CO with A_v presented by de Jong, Dalgarno, and Boland 1980 or Gerola and Glassgold 1978). In this case $\partial P/\partial r > 0$, and the cloud experiences an inward pressure gradient force that assists gravity in producing collapse. If the inward pressure gradient force is strong, then the previously experienced difficulties in collapsing low solar mass clouds from their initial diffuse stage are altogether avoided, at least in the level of approximation of negligible rotation and turbulence. Clearly, it is important to use a representation of the temperature structure that incorporates all essential physics. The present study does this using a new, entirely semiempirical approach.

a) Parameterization of Temperature

The temperature distribution in a collapsing cloud should be obtained by simultaneously solving the hydrodynamical equations and the heat balance equation:

$$\frac{\partial u}{\partial t} = \frac{P}{\rho}\frac{\partial \rho}{\partial t} + \Sigma_i \Gamma_i - \Sigma_j \Lambda_j\ , \tag{6}$$

where u is the internal energy and Γ_i the heating rate due to the ith physical process (i.e., photoelectron heating, cosmic-ray heating, chemical heating, H_2 formation, and photodissociation heating) and Λ_j is the cooling rate due to the jth coolant, such as C^+, C, and CO. Ideally, the heat balance equation should be solved simultaneously with chemical balance equations because concentrations of C^+, C, and CO and the magnitude of chemical heating are controlled by chemistry. Current understanding of heating and cooling processes, however, considerably underpredict the temperature of diffuse

clouds (i.e., theoretical $T = 40.2$ K for $A_v \simeq 0$ and $n_H = 142$ cm^{-3} from de Jong, Dalgarno, and Boland 1980, as compared with observed values significantly in excess of 100 from Savage *et al.* 1977 or Jura 1975*a*). Furthermore, even if all heating and cooling processes were precisely known, simultaneous solution of the hydrodynamical, thermal, and chemical equations would still be of limited usefulness in this study because the computational cost of such solutions would severely limit our ability to run modeling experiments to study the effects of uncertainties in other physical processes. Consequently, a semiempirical approach was adopted which contains essential physics of heating and cooling. The heating was assumed to be due to photoelectrons from the grains and cosmic rays. The cooling was assumed to be due to a fictitious two-level coolant whose characteristic remains unaffected by $C^+ \rightarrow C \rightarrow CO$ conversion. These semiempirical assumptions enabled us to write

$$\Sigma_i \Gamma_i = (a + be^{-cA_v})n_H \quad (7)$$

and

$$\Sigma_j \Lambda_j = de^{-\alpha/T} n_H^2 , \quad (8)$$

so that

$$T = \alpha/[\beta + \ln n_H - \ln (1 + \gamma e^{-cA_v})] \quad (9)$$

under thermal equilibrium, which was assumed to prevail through the collapse because heating and cooling time scales are generally much smaller than dynamical time scales. The occurrence of the constants a, b, c in equation (7) follows directly from the discussions of the cosmic-ray and grain photoelectron heating presented by Gerola and Glassgold (1978) and de Jong, Dalgarno, and Boland (1980). For example, the constant c depends upon the transfer of the interstellar radiation involved in photoelectron heating and has the value 1.8 according to de Jong, Dalgarno, and Boland (1980). The constants d and α of equation (8) depend upon level separation and transition probability, and the constants β and γ of equation (9) are functions of a, b, and d. Semiempirical equation (9) makes the temperature a function of n_H and A_v and decouples thermal balance from chemistry. The feasibility of our approach was verified by the fact that, with suitable choices of constants, equation (9) is capable of reproducing, with an accuracy of 10% or better, the temperature derived from elaborate theoretical calculations, such as those of de Jong, Dalgarno, and Boland (1980), in which abundances of C^+, C, and CO were derived from the solution of a large set of chemical equations, and their contributions to cooling from a consideration of all relevant energy levels and radiative transfer effects. Sample results of the test are given in Table 1 for $\alpha = 163$, $\beta = 2.5$, $\gamma = 50$, and $c = 1.8$. Since the range of C^+, C, and CO abundances encountered in de Jong, Dalgarno, and Boland's (1980) calculations are similar to the abundances which we would encounter in our study, the empirical assumption of replacing C^+, C, and CO coolants by a fictitious coolant and the resulting equation (9) were deemed adequate for our purpose.

Having thus verified our semiempirical approach, we adjusted the constant γ in equation (9) to a value of 500 to reproduce observed diffuse cloud (e.g., 139 Tau, ξ Per, α Cam, ζ Oph) temperatures (Jura 1975*b*) within a factor of ≤ 2. The upward adjustment of γ reflects the cumulative effect of current uncertainties in the strength of the interstellar radiation field, photoelectron heating efficiency, the energy of the photoelectrons, and other parameters. A factor of 2 accuracy was considered reasonably good because of the uncertainties in the observationally derived temperatures. The dense-cloud temperatures, being insensitive to γ, remained in good agreement (10% or better) with observations (Wootten *et al.* 1978). The resulting equation for T in terms of A_v and n_H was

$$T = 163/\{2.5 + \ln n_H - \ln [1 + 500 \exp (-1.8A_v)]\} . \quad (10)$$

Although most of the present calculations were done with equation (10), we also experimented with the following two equations:

$$T = 163/\{2.5 + \ln n_H - \ln [1 + 500 \exp (-1.8A_v)]\} + 10 \ln (1 + 5.0 \times 10^{-6} n_H) \quad (10a)$$

and

$$T = 163/\{2.5 + \ln n_H - \ln [1 + 250 \exp (-1.2A_v)]\} . \quad (11)$$

Equation (10a) mimics an increase in temperature with increasing density in the cores of dense clouds observed by Wootten *et al.* (1978). Equation (11), on the other hand, represents a decrease in T with A_v less steep than that given by equation (10) and is suggested by a three-parameter (β, γ, and c) fit of the observed temperature (note that eq. [9] was only a two-parameter [β and γ] fit by holding $c = 1.8$ on the basis of de Jong, Dalgarno, and Boland 1980).

As pointed out earlier, the semiempirical formula was desirable because current versions of *ab initio* calculations have great difficulties in predicting the observed temperature of diffuse clouds, and because the semiempirical formula significantly reduces the computational burden. Nevertheless, the formula has certain disadvantages. Elimination of the abundances of the various coolants in the temperature formula implies that the chemical time scales for the important coolants are short relative to the dynamical time scale. This implication may not be always true. Furthermore, the use of the empirical

TABLE 1

COMPARISON OF TEMPERATURES DERIVED FROM SEMIEMPIRICAL FORMULA (9) WITH THOSE DERIVED FROM FIRST PRINCIPLES[a]

PHYSICAL PARAMETERS		DERIVED TEMPERATURES (K)	
A_v (mag)	n_H (cm^{-3})	From Formula (9)	From First Principles[a]
0	1.42 + 2[b]	46	40
0	5.66 + 2	33	28.6
0.1	3.40 + 3	24	24
0.1	1.36 + 4	20	23.3
0.25	8.21 + 3	20	22.0
0.25	3.28 + 4	17	22.5
0.5	1.60 + 4	18	20
0.5	6.41 + 4	16	22.2
1.0	3.09 + 4	15	17
1.0	1.23 + 5	14	22.5
2.0	5.75 + 4	13	13
2.0	2.30 + 5	12	15.9
4.0	9.85 + 4	12	9
4.0	3.94 + 5	11	10.4
8.0	1.31 + 5	11	10
8.0	5.25 + 5	10	11.9

[a] De Jong, Dalgarno, and Boland 1980.
[b] $1.42 + 2 \equiv 1.42 \times 10^2$.

formula also suppresses any possible role of thermal-chemical instabilities in the dynamics of the cloud.

b) *Treatment of* $H \rightarrow H_2$ *Conversion*

As pointed out earlier, $H \rightarrow H_2$ conversion affects the dynamical evolution through the occurrence of the mean molecular mass μ in equation (3). In addition, this conversion is of prime importance for chemistry because most chemical reactions are initiated by H_2 formation (see, e.g., flow diagrams presented by PH). Our treatment of $H \rightarrow H_2$ conversion was therefore designed to reproduce observations as well as possible. As usual, we assumed H_2 formation to take place on grains with a rate coefficient of 3×10^{-17} cm^3 s^{-1} (Jura 1975*b*). The treatment of the H_2 photodestruction rate is, however, more complicated because of the H_2 self-shielding effect in the radiative transport of the Lyman and Werner band photons. The need for a computationally fast scheme led us to adopt de Jong, Dalgarno, and Boland's (1980) H_2 photodissociation rate. We recognize that this expression neglects photodissociation from the $J > 1$ levels of $v'' = 0$ and from $v'' > 0$ states together with the contributions of Werner bands. In the light of the results of Federman, Glassgold, and Kwan (1979) and Joshi (1978), it is easy to see that de Jong, Dalgarno, and Boland's (1980) expression may significantly underestimate the H_2 photodissociation rate. We also recognize that there may be uncertainties in the simplified H_2 formation rate as well. We have tried to compensate for these deficiencies in a semiempirical manner by attaching a lumped correction factor to the H_2 photodissociation rate. The fact that the semiempirically modified photodestruction rate gives a better representation of the observed variation of $N(H_2)$ with N_H (Bohlin, Savage, and Drake 1978) is seen from Figure 1. The inferred densities of many of these clouds are close to 100 cm^{-3} or more (Jura 1975*a*, *b*). At this density, de Jong, Dalgarno, and Boland's (1980) photodissociation rate, and the adopted H_2 formation rate (3×10^{-17} cm^3 s^{-1}) gives a higher $N(H_2)$ than was observed (see the dashed curve in Fig. 1). In contrast, the use of a semiempirical correction factor of 5 for the photodissociation rate gives much better agreement with observation (see the continuous curve).

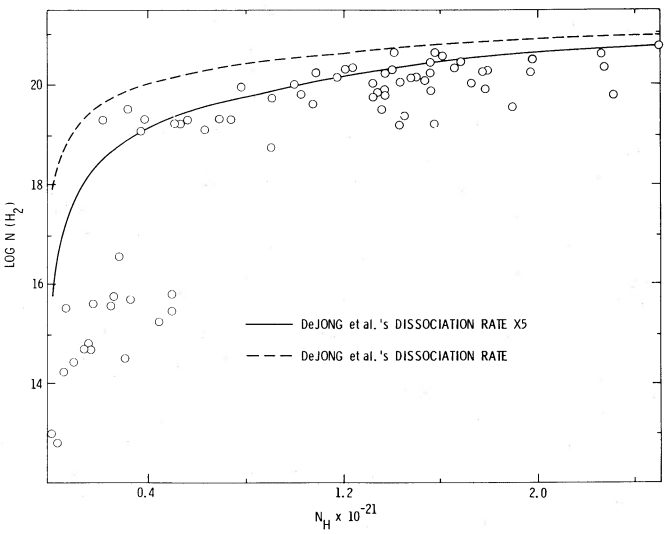

FIG. 1.—Theoretical and observed variations of $N(H_2)$ with N_H. Circles represent the observed data. The solid and dashed lines show theoretical results using $n_H = 100$ cm^{-3} and photodissociation rates as noted in the figure.

c) *Treatment of the Chemistry of* H-C-N-O *Molecules*

The use of our semiempirical formulae (eqs. [10], [10a], and [11]) decouples chemical evolution from the dynamical evolution. The chemistry of H-C-N-O–bearing molecules in our study was, therefore, studied independently, utilizing the values of ρ and T as functions of the radial distance r and time t as derived from the dynamical part of the calculations. We considered 91 H-C-N-O–bearing atoms, molecules, and positive ions. These 91 species are exactly the same as those considered by PH—excluding, of course, the negative ions and sulfur and silicon families of species that were also considered in PH. Furthermore, all metals are lumped together symbolically as M and M^+ and were given photoionization properties similar to those of silicon. The initial abundances of M and M^+ were, however, much smaller than those used by PH. This was necessary to ensure that the electon densities in the dense clouds agreed with observations. Relevant gas-phase reactions of our 91 H-C-N-O–bearing species were also the same as those used by PH, except for the changes in the reaction rate coefficients mentioned in Table 2. In other words, the gas-phase chemical reactions of our 91 species were extracted from the list in PH by first eliminating the reactions of negative ions, metals, and sulfur and silicon families, and then introducing the changes in the rate constants mentioned in Table 2. Reported rate constants of the radiative association reactions, $C^+ + H_2 \rightarrow CH_2^+ + h\nu$ and $CH_3^+ + H_2 \rightarrow CH_5^+ + h\nu$, span a very wide range of values, e.g., 10^{-15}–10^{-11} cm^3 s^{-1} at 10–20 K for the radiative association of CH_3^+ with H_2 (Herbst 1983, 1980*a*, *b*, 1976; Adams and Smith 1981; Smith and Adams 1978). Guided by the theoretical studies of Bates (1983, 1980), we have generally used the lower values. Depletion of neutral species by condensation onto the grains was assumed to occur with a 50% probability at every collision with grains. The rates at which gas-phase molecules collide with the grains were determined by means of a very simplified formula such as that used by Iglesias (1977). (Laboratory measurements of Barlow, Dunn, and Schauer 1984, reported after the completion of the present study, indicate a significantly higher rate coefficient for the radiative association of C^+ and CH_3^+ with H_2. Also, further studies by Langer and coworkers [W. D. Langer 1984, private communication] have confirmed the importance of CO self-shielding first pointed out by Bally and Langer 1982 in the context of isotope-selective photodestruction of CO. Accurate f-values for the discrete transitions of CO are, however, not well established at this time, and the problem of CO self-shielding is further complicated by possible overlap between the absorption bands of CO and H_2 [Bally and Langer 1982]. It is important to mention these new developments because the present work used low rate coefficients for the radiative associations of C^+ and CH_3^+ with H_2 and neglected the CO photodissociation by line radiation and by the ultraviolet generated deep inside dense clouds by cosmic-ray excitation of H_2.)

III. NUMERICAL ALGORITHMS AND INITIAL CONDITIONS

The hydrodynamical part of our calculations was done by a computer code developed by Bodenheimer (1968), with a modification for the new functional dependence of T on n_H and A_v. Because the code has been described in considerable detail by Bodenheimer (1968), no further discussion of the numerical technique will be presented here. We would, however, like to

TABLE 2

LIST OF REACTIONS WHOSE RATE COEFFICIENTS HAVE BEEN MODIFIED FROM THE PREVIOUS STUDY

	Reaction	Old Rate[a]	New Rate	Reference
1.	$O^+ + O_2 = O_2^+ + O$	3.0E−12[b]	2.0E−11	1
2.	$CH^+ + O_2 = HCO^+ + O$	4.8E−10	9.7E−10	1
3.	$OH^+ + CH_4 = H_3O^+ + CH_2$	3.0E−11	1.3E−9	1
4.	$OH^+ + CO = HCO^+ + O$	1.0E−9	2.0E−11	1
5.	$CO^+ + H_2O = HCO^+ + OH$	4.2E−10	8.8E−10	1
6.	$CO^+ + H_2O = H_2O^+ + CO$	4.2E−10	1.7E−9	1
7.	$CH_2^+ + O_2 = HCO^+ + OH$	4.7E−10	9.1E−10	1
8.	$CH_2^+ + H_2O = H_3CO^+H$	5.2E−10	1.2E−9	1
9.	$HCO^+ + H_2O = H_3O^+ + CO$	2.7E−9	3.2E−9	1
10.	$NH_3^+ + H_2 = NH_4^+ + H$	1.7E−11 exp (−1044/T)	1.0E−13	1
11.	$CH_4^+ + H_2O = H_3O^+ + CH_3$	9.6E−10	1.5E−9	1
12.	$N + NO = N_2 + O$	8.2E−11 exp (−410/T)	3.4E−11	1
13.	$C^+ + H_2 = CH_2^+ + h\nu$	6.0E−16	1.0E−16	2
14.	$CH_3^+ + H_2 = CH_5^+ + h\nu$	1.0E−15	3.0E−15	2
15.	$C^+ + NH_2 = HCN^+ + H$	1.1E−9	5.5E−10	3
16.	$C^+ + CH = CH^+ + C$	3.8E−10	1.0E−9	3
17.	$C^+ + CH = C_2^+ + H$	3.8E−10	1.0E−9	3
18.	$CH_3^+ + C = C_2H^+ + H_2$	1.2E−9	5.0E−10	3
19.	$C_2H_2^+ + O = C_2HO^+ + H$	6.5E−10	1.3E−9	3
20.	$C + NH = CN + H$	1.0E−10(T/300)$^{1/2}$	5.0E−11(T/300)$^{1/2}$	3
21.	$N + CH = CN + H$	5.0E−11(T/300)$^{1/2}$	2.5E−11(T/300)$^{1/2}$	3
22.	$CH_2 + O = HCO + H$	2.0E−12(T/300)$^{1/2}$	5.0E−12(T/300)$^{1/2}$	3
23.	$CH_2 + N = HCN + H$	2.0E−11(T/300)$^{1/2}$	1.0E−11(T/300)$^{1/2}$	3

NOTES.—(1) From Huntress *et al.* 1980. (2) See § II*c*. (3) The new rate coefficients represent our preference only.

[a] Prasad and Huntress 1980*a*.

[b] 3.0E−12 ≡ 3.0 × 10^{-12}, and so on.

add that A_v was calculated by a direct numerical integration of the radial density distribution, i.e.,

$$A_v(r, t) = 223 \int_r^R \rho(r, t)dr \,, \qquad (12)$$

where R is the radius of the cloud at the time t. The numerical coefficient is for a hydrogen mass fraction of 0.74 and $N(\mathrm{H})/A_v = 2 \times 10^{21}$ (Jenkins and Savage 1974). Also, A_v determined from time step t_{n-1} was used in the step t_n. The smallness of the time interval used ensured that the error due to this approximate way of treating current A_v was negligible.

The chemistry was studied by the same code as was used by PH. Since this code is also described with adequate detail in PH, no further discussion is needed here except that the H_2 photodissociation rates used by PH were modified as described in the discussion presented in § II*b*. Also, only a limited number of species and chemical reactions were used in the present work.

At any specified time step in the evolution, the chemistry code was run at 12 mass points $m_1, m_2, \ldots, m_{11}, m_{12}$. The first mass point ($m_1$) was always at the surface, and the last mass point (m_{12}) was always at the center of the cloud. In the Lagrangian formulation of the hydrodynamical collapse problem, values of mass points may range from zero to one, respectively, at the center and the surface. These values of the mass points signify the fraction of the total mass of cloud which is interior to that point. In essence, mass points in Lagrangian formulation are equivalent to radial distance in Eulerian formulation (see, for example, review papers on hydrodynamical collapse cited in the introduction). The radial distance from the center of any mass point decreases as the collapse progresses. We keep track of this variation, so that ultimately the results of calculations may be displayed as functions of radial distances.

The visual extinction (A_v) at each mass point was calculated from equation (12), so that $A_v = 0$ at the first mass point located at the surface at all times. The 12 mass points were selected in such a manner that values of n_{H} and A_v at any mass point did not vary by a factor greater than 2 relative to their values at neighboring mass points at any time. Time steps ran from time $t = t_0 = 0$ to $t = t_1$ from t_1 to t_2 to $t_3, \ldots$, from t_{14} to t_{15}, where at $t = t_{15}$ (usually a few times 10^6 years) the central density attains values of a few times 10^6 cm^{-3} (see Table 3). The length of a time step was such that values of n_{H} and A_v at any mass point did not change appreciably compared with their values at the beginning of that time step. All matter was assumed in atomic form at each mass point at the beginning of the first time interval. With these initial conditions the chemical code was run at each mass point for time $t = t_1 - t_0$, keeping n_{H} and A_v fixed at their values appropriate for the beginning of the time step. The effect of variation in n_{H} due to gravitational contraction during this chemistry step was taken into account at the end of the step by multiplying the number densities of each species at each mass point m_i (i = 1, 2, ..., 11, 12) by the factor $[(n_{\mathrm{H}})_{t=t_1}/(n_{\mathrm{H}})_{t=t_0}]$ appropriate for that mass point. The multiplicative factor itself is known from the hydrodynamical calculation performed in advance of the chemistry calculation. This type of approximate method for incorporating the effects of dynamics on chemistry has been widely used with considerable success in studying physically similar environments, such as cometary comae where the gas is expanding outward (see Mitchell, Prasad, and Huntress 1981; Giguere and Huebner 1978). Values of A_v for each mass point are also updated at this time. The new values of species density and A_v at time $t = t_1$ then serve as the initial conditions for the chemistry code to be run from time $t = t_1$ to $t = t_2$, and the whole process is repeated until t_{15} is reached.

TABLE 3

SELECTED PHYSICAL CHARACTERISTICS OF THE MODEL CLOUDS

PHYSICAL PROPERTY	MODEL							NOTES
	A	B	C	D	E	F	G	
Mass ($M_\odot$)	1000	1000	100	100	100	100	40	
Initial density (g cm^{-3})	1.65E−22	3.30E−22	3.30E−22	3.30E−22	3.30E−22	...	3.30E−22	1
Surface pressure (dynes cm^{-2})	2.68E−12	2.54E−12	2.68E−12	2.54E−12	1.67E−12	2.54E−12	2.66E−12	
Temperature formula	10	10	10	10a	11	10	10	
Initial visual extinction (A_v)	0.5	0.8	0.4	0.4	0.4	0.6	0.28	2
Free-fall time (yr)	5.15E6	3.86E6	3.86E6	3.86E6	3.86E6	3.86E6	3.86E6	
$t_{0.5}$ (yr)	...	...	1.20E6	1.20E6	1.89E6	...	1.86E6	3
$t_{1.0}$ (yr)	2.73E6	1.64E6	2.04E6	2.04E6	2.92E6	1.99E6	2.78E6	
$t_{1.5}$ (yr)	3.11E6	2.19E6	2.32E6	2.32E6	3.24E6	2.33E6	3.20E6	
$t_{2.0}$ (yr)	3.37E6	2.57E6	2.45E6	2.65E6	3.47E6	2.51E6	3.37E6	
t_4 (yr)	3.93E6	3.16E6	2.54E6	2.57E6	3.63E6	2.68E6	3.50E6	4
t_5 (yr)	4.07E6	3.32E6	2.81E6	2.81E6	3.90E6	2.94E6	3.93E6	
t_6 (yr)	4.10E6	3.33E6	2.88E6	2.90E6	3.40E6	3.02E6	4.07E6	

NOTES.—(1) 1.65E−22 ≡ 1.65×10^{-22}, and so on. Also, model F has constant pressure, rather than constant density, as the initial condition. Initial density in model F therefore varies with radial distance to keep pressure constant. (2) Visual extinctions are through the center of the clouds. (3) First four t-values: the time in years at which the visual extinction through the center of the clouds attained the value indicated by the subscript. (4) Last three t-values (t_n): the the time in years at which the central densities of clouds attained the value 10^n (approximately).

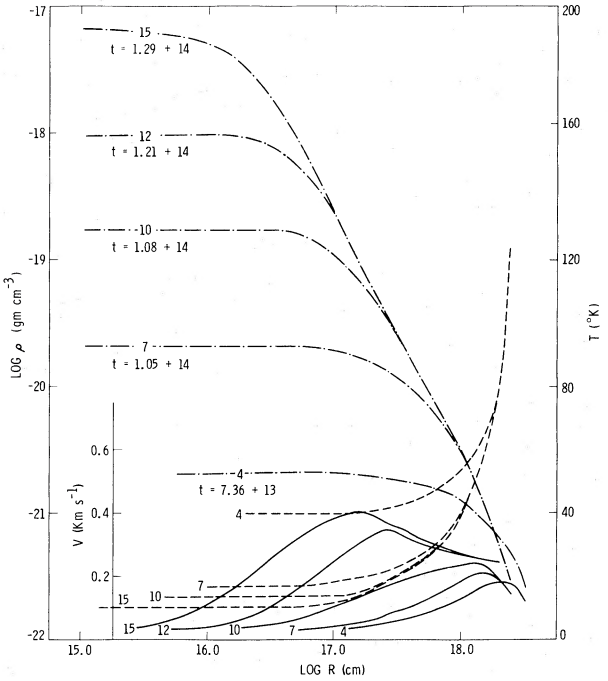

FIG. 2.—Evolution of density (*dot-dash lines*), temperature (*dashed lines*), and velocity (*solid lines*) distributions as a function of radial distance for a cloud of 40 $M_\odot$ and initial density of 3.3×10^{-22} g cm^{-3}. Increasing numerals allotted to the curves indicate the progress of evolution in time. The times, such as $1.29 + 14 \equiv 1.29 \times 10^{14}$ s, are indicated on the density curves only.

IV. RESULTS AND DISCUSSION

a) Dynamical Evolution

We have considered the hydrodynamical and chemical evolution of a number of spherically symmetrical models of clouds with different masses, initial densities, and temperature–density–A_v relations. Distributions of density, temperature, and velocity as functions of the radial distance within a cloud for different states of evolution of a 40 $M_\odot$ cloud with initial density 147 cm^{-3} are shown in Figure 2. This model is taken as a representative of the situation encountered in low-mass clouds. The density increase with contraction is more rapid near the center of the model cloud than in its outer layers because of the requirement of constant pressure (and density) at the surface. Consequently, the model cloud develops a nearly uniform high-density core surrounded by an envelope in which density varies as r^{-p}. Although the value of p may differ in different parts of the envelope, its mean value, $\bar{p}$, averaged over the entire envelope ranges between 1.5 and 2.0 for the clouds under consideration here. Other conditions remaining the same, p increases with the cloud mass. As noted by Bodenheimer and Sweigert (1968), the edge of the core retreats inward (in radius and mass) with a velocity equal to the sum of the local collapse and the sound velocities. The mass fraction inside the core therefore diminishes with time. The collapse velocity increases nearly linearly with the radius in the core but decreases approximately as $r^{-0.5}$ in the envelope. Thus the velocity does not have a simple monotonic form as is assumed in many studies of cloud collapse. The collapse velocities in our models are within the range of velocities inferred from the observed line widths in dark clouds.

Although the above-mentioned characteristics of the density and velocity distributions are quite similar to those obtained for isothermal collapse (Bodenheimer and Sweigert 1968), the temperature distributions in our models are markedly different. Temperature increases from the center to the surface even during the initial phases of the collapse. At the later stages T decreases with time at the interior points as ρ and A_v increase. Temperature becomes nearly uniform within the dense opaque core but increases sharply in the outer layers of a cloud (see Fig. 2). An important property of this more realistic initial temperature distribution is that it has enabled us to collapse even warm (60–80 K) low-mass (~ 40 $M_\odot$) diffuse clouds. Under isothermal conditions the collapse of such clouds cannot continue indefinitely because the thermal energy E_T may exceed the gravitational energy E_G in these clouds. In contrast, they can collapse under our temperature distribution because the inward pressure gradient force assists gravity in producing the collapse, as was mentioned briefly in § II*a*. The initial positive pressure gradient ($\partial P/\partial r > 0$) disappears on the time scale of sound travel across the cloud. This is, however, of little consequence in the continued collapse of the cloud, because the density increase and cooling that occur during that time period cause E_G to exceed E_T.

Other effects of the temperature structure persist throughout the evolution. Near the surface of our models, the density varies more steeply than in isothermal models because of the rapid variation of A_v and T. Also, collapse times are less than for isothermal models, because of the initial pressure acceleration and because in evolved models the negative pressure gradient opposing collapse becomes smaller with outwardly increasing temperature. The collapse times of our models are slightly less than the initial free-fall times.

Although the above general features apply to all of our models, the dynamical evolution depends in detail on the mass, the initial density, and the form of the T–ρ–A_v relation. This is obvious from the data presented in Figures 3 and 4 and in Table 3. The largest differences result from varying the mass. A large and massive core persists during the collapse of the 1000 $M_\odot$ cloud (Fig. 3) because the sound crossing time, t_s, exceeds the collapse time, t_c. In the smaller and warmer 40 $M_\odot$ cloud, however, $t_s \approx t_c$, and the density profile becomes quite steep by the last epoch (*d*) shown in Figure 3. The time to reach a specified density is not, however, a simple function of the mass. Low-mass clouds have initially a significant pressure force assisting collapse, but also at later times a larger pressure force opposing collapse. Total collapse time is therefore a minimum for clouds of intermediate mass ($M = 100$ $M_\odot$ in Table 3). However, the time scale for collapse varies by less than a factor of 2 over the range of mass considered here. The collapse velocity within a model scales roughly with the ratio of the initial cloud size to the collapse time. The more massive models attain higher velocity because radius increases with mass more rapidly than does collapse time.

The principal effects of varying the initial density are illustrated by the two 1000 $M_\odot$ models A and B in Table 3. Model A, with low density, has a larger collapse time, consistent with the larger free-fall time scale, $t_{ff} \sim \rho^{-1/2}$, although the collapse time increases more slowly than t_{ff} because of the larger surface temperature and initial pressure acceleration in the low-density model. The larger pressure at low density also allows less massive models to collapse. The minimum mass for collapse is found to be 40 $M_\odot$ for $\rho = 3.30 \times 10^{-22}$ g cm^{-3} and 20 $M_\odot$ for $\rho = 1.65 \times 10^{-22}$ g cm^{-3}. The structure profiles of models starting with different initial density are, however, quite

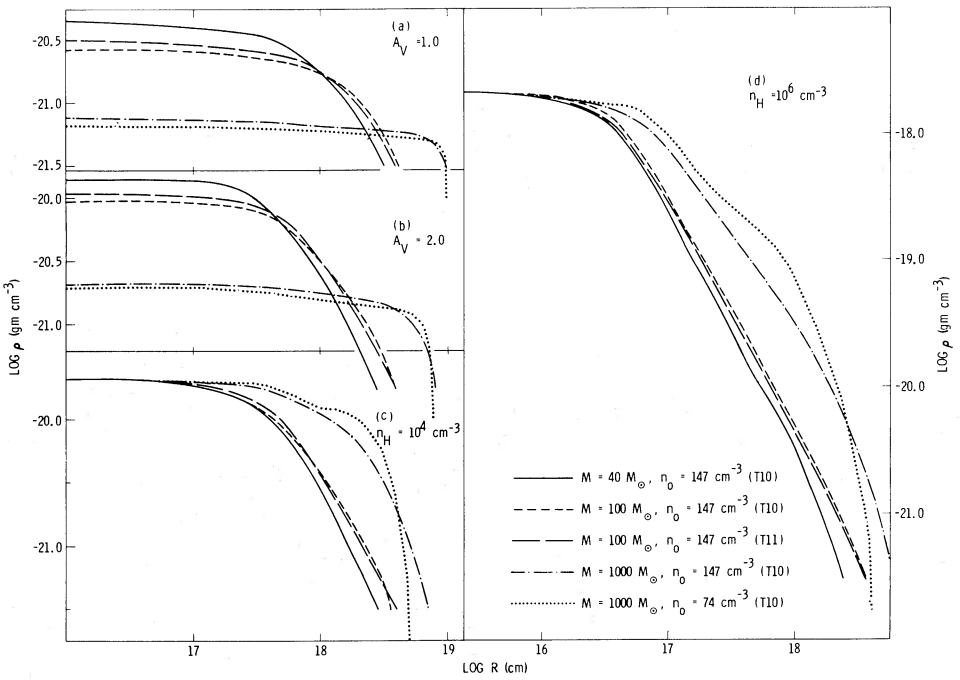

FIG. 3.—The effect of mass, initial density, and temperature formula on the density structure of dynamically evolving clouds at different stages of their evolution. Parts *a* and *b* depict the diffuse state (visual extinction through the center, $A_v = 1.0$ and 2.0, respectively). Parts *c* and *d* represent the dense state when the density at the center n_H^c reached 10^4 and 10^6 cm^{-3}, respectively. Right-hand side *Y*-axis should be used with part *d* only. *T10* and *T11* refer to temperature formulas (10) and (11).

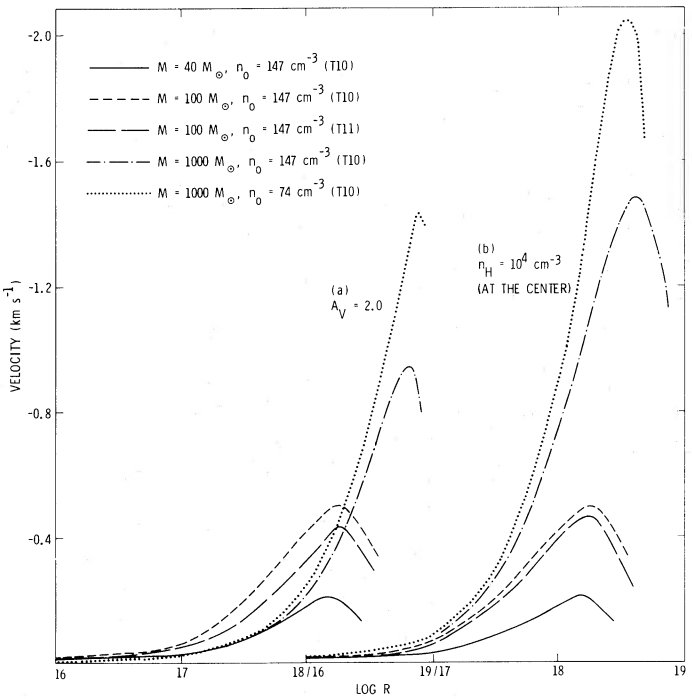

FIG. 4.—The effect of mass, initial density, and temperature formula on the velocity structure of a dynamically evolving cloud at a diffuse (*a*) and a dense (*b*) state

similar. This is easily seen by comparing appropriate curves in Figures 3 and 4.

Mass and initial density remaining the same, use of temperature formula (10) produces a faster collapse than that resulting from the use of temperature formula (11). This is a direct consequence of the greater inward pressure gradient force generated in models that obey equation (10). The model cloud C therefore takes less time to attain a specified A_v or a specified central density compared with the model cloud E of the same mass and initial density (see Table 3, cols. [4] and [6]). Collapse velocity is also consistently higher for the models with temperature formula (10) than for the models with formula (11). Figure 4*a* shows this effect.

Our model clouds spend most of their lives in a diffuse state ($A_v \lesssim 2$). Once the core becomes dense ($\sim 10^3$–10^4 cm^{-3}), its collapse is extremely fast. The evolutionary time scale of dense clouds (defined here as the time taken to change the core density by a factor of e [$= 2.7$]) decreases very rapidly with increasing density. As a corollary, the number of clouds with a given density should decrease significantly as the density increases. This is consistent with observations described by Lynds (1962). According to Lynd's data, the ratio of the number (n_1) of clouds of type 1 to the number (n_6) of clouds of type 6 is about 3. This ratio n_1/n_6 is obtained by considering the areas obscured by these clouds (Table 3 of Lynds 1962) and the sizes of these clouds (Table 5 of Lynds). Tentatively identifying type 1 clouds as clouds with $A_v = 1$ and type 6 clouds as clouds with central density $= 10^4$ cm^{-3}, the theoretical value of the ratio n_1/n_6 is approximately equal to $\Delta t_1/\Delta t_6$, where Δt is the time needed to change A_v or the central density (as appropriate) by a factor of e ($= 2.7$). Thus, the theoretical value of the ratio n_1/n_6 ranges from 3 to 14, depending upon the cloud mass and the initial density (see Table 3). The present theory is therefore not inconsistent with Lynds's data.

One test of the theory of cloud evolution presented here is that it should predict star formation at a rate consistent with observational evidence. A well-known difficulty with the assumption that all material within the molecular clouds of our Galaxy is collapsing at near free-fall velocity is that the star formation rate would be at least an order of magnitude larger than the currently accepted value (Zuckerman and Palmer 1974; Field 1978; Smith, Biermann, and Mezger 1978). Careful examination of our models shows, however, that only a small fraction of the total cloud mass attains the high density and low temperature needed to initiate star formation. (Between the two most evolved models shown in Fig. 2 changes in density and temperature occur with only the central 3% of the cloud material.) Thus the premise that the majority of the interstellar clouds are collapsing and may eventually form stars may well be plausible because the efficiency with which interstellar matter is converted into stellar matter appears to be small.

b) Chemical Evolution

We will now discuss the chemistry in our model clouds as they evolve from diffuse to dark states. For clarity the discussion will be limited to three clouds with mass 40, 100, and 1000 $M_\odot$ and initial density $\rho_0 = 3.3 \times 10^{-22}$ g cm^{-3}. At early times the clouds are diffuse and the dynamical time scales (t_d) are large (i.e., $t_d = 3 \times 10^{13}$ s for a change in A_v from 0.5 to 1 due to contraction). In comparison, the photochemical time scales (t_{pc}) are much shorter, typified by photodissociation-photoionization rate coefficients of about 10^{-11}–10^{-12} s^{-1} at $A_v = 0.5$–1. At early times, therefore, the collapsing clouds are in photochemical equilibrium. This result implies that the choice of initial chemical composition (i.e., initial abundances of H_2, C, C^+, CO) has little effect on the chemical composition of later evolved stages. Gerola and Glassgold (1978), however, expressed the opposite viewpoint with respect to the importance of the initial chemical composition. The key point is that Gerola and Glassgold's (1978) model cloud with $A_v = 2$ and $m = 2.5 \times 10^4$ $M_\odot$ was not in photochemical equilibrium throughout initially. Indeed, Gerola and Glassgold (1978) themselves remarked that by choice of the initial chemical composition they were fixing the early history of the cloud. In the present work we have avoided this problem by starting early enough in the evolutionary history of our model clouds.

As the collapse progresses, clouds become dense and dark. The dynamical time scale decreases approximately as $\rho^{-1/2}$. Photochemical time constants, on the other hand, increase exponentially with increasing A_v, so that very soon the photochemical time constant loses its significance. At this stage we may define a chemical time constant t_c associated with ion-molecule and neutral reactions. At any given n_H the magnitude of the chemical time constant t_c of a species is quite sensitive to the chemistry of that species. The chemical time constant, therefore, may vary over a few orders of magnitude from one species to another. The dynamical time constant is, however, chemistry-independent in the present model, mainly because of the use of the semiempirical temperature formula. Thus, the relative importance of dynamical compression and chemistry in determining the abundance of any chemical species is highly species-dependent at any given evolutionary epoch. To complicate the matter further, the relative importance of compression and chemistry for any given species depends upon n_H because $t_d \propto \rho^{-1/2}$ and $t_c \propto \rho^{-1}$. In other words, if for any given n_H dynamical compression is relatively more important in determining the abundance of any species, the reverse may be true for the same species at another suitably higher n_H.

The evolution of C^+, C, and CO distributions in our 40 and 1000 $M_\odot$ clouds is shown in Figures 5 and 6. At all stages of evolution, C^+ is the most abundant species in the photoionization-dominated outer regions of small A_v and the least abundant in the cosmic-ray ionization–dominated inner regions of large A_v. On the other hand, the relative abundances of C and CO in the inner region as well as in the C^+ to (C + CO) transition zone is quite sensitive to the cloud mass and the stage of evolution. The details are obvious from Figures 5*a*–5*d* and 6*a*–6*d*. A particularly noteworthy feature is that in the 40 $M_\odot$ cloud the conversion is from C^+ to CO without C ever dominating the C^+, C, and CO abundances. In more massive clouds, however, there is always an epoch beyond which n(C) becomes greater than both $n(C^+)$ and n(CO) in some region or other. In the case of 1000 $M_\odot$ that epoch is roughly when the central density becomes $\geq 10^3$ cm^{-3}. The extent and the location of the region over which C dominates in the cloud are of course time-dependent. Introduction of self-shielding effects in CO photodissociation will certainly change the details of the C^+, C, and CO distribution in dynamically evolving clouds. Nevertheless, the basic conclusion that N(C)/N(CO) may be dependent on cloud mass and evolutionary time is not expected to change. Observationally, N(C)/N(CO) does vary considerably from cloud to cloud (Phillips and Huggins 1982). The present study provides an additional means of understanding the observed variation of this ratio. Another noteworthy feature is the significant

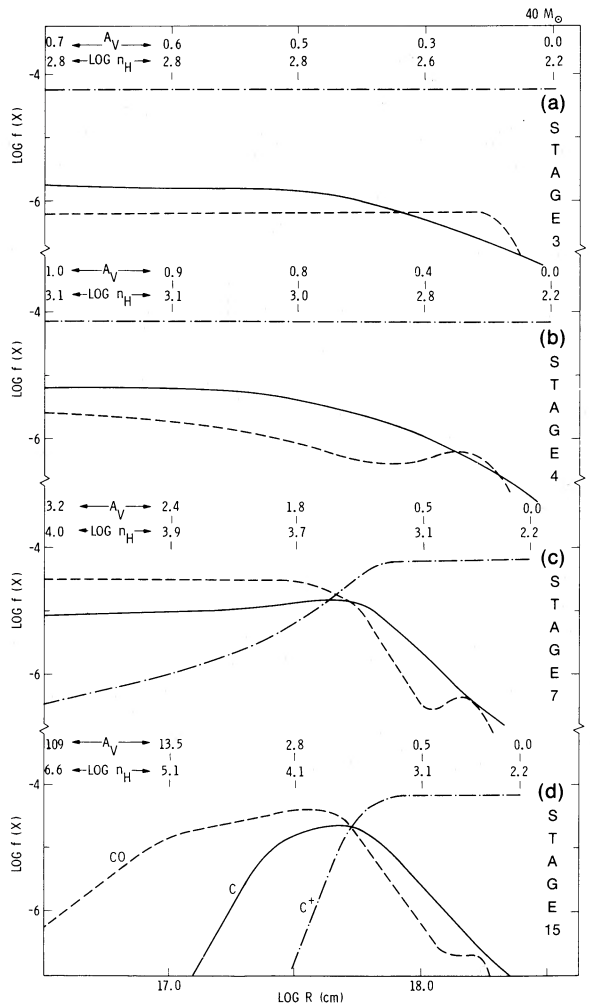

FIG. 5.—Distribution of the fractional abundances of C^+ (*dot-dash lines*), C (*solid lines*), and CO (*dashed lines*) at different stages of evolution (*a–d*) for a cloud of 40 $M_\odot$ and an initial density of 147 cm^{-3}. The two rows of numbers on the top of each section represent the distribution of A_v and n_H across the cloud along a line of sight passing through the center.

decrease of the fractional abundances f_{CO} and f_C of both CO and C ($f_{CO} = n(CO)/n_H$ and $f_C = n(C)/n_H$) in the core of clouds when they become very dark ($A_v > 10$) and very dense (core densities $\sim 10^5$–10^6 cm^{-3}; see Figs. 5*d* and 6*d*). The decrease in f_{CO} is due to the introduction of condensation onto grains, and the steeper decrease in the core of f_C is due to the additional effect of C → CO conversion.

Figures 5 and 6 give much more detail than is observationally verifiable. For example, in the case of clouds observable in the ultraviolet the measured quantities are the column densities and A_v along the line of sight; information about local n_H and A_v is totally smeared. In Figure 7, therefore, we present the theoretical column densities of carbon, N(C), as a function of the visual extinction looking through the center of our model clouds as they evolve from their diffuse to dark states and thereby span a large range of A_v. Theoretical results are for clouds of 40, 100, and 1000 $M_\odot$, starting with $\rho_0 = 3.3 \times 10^{-22}$ g cm^{-3}. Observational data are from *International Ultraviolet Explorer* (*IUE*) observations (Jenkins, Jura, and Loewenstein 1983) for low A_v (diffuse) clouds and from radio observations (Phillips *et al.* 1980; Phillips and Huggins 1982; Frerking *et al.* 1984) for dense clouds (high A_v). The data of Phillips *et al.* (1980) have been lumped together and have arbitrarily been shown at $A_v = 16$. This is possible because the theoretical curves become flat in this region of A_v. The agreement between the theoretical curves for low-mass (40–100 $M_\odot$) clouds and the observations is quite satisfactory in the region of A_v, where the two overlap. Observational data, therefore, appear to support our thesis that the same mass of gravitationally unstable interstellar gas may appear as clouds of different A_v and N(C) as it evolves from a diffuse to a dense state. In other words, many—if not all—interstellar clouds may be dynamically evolving. In principle, simple constant density–constant temperature equilibrium models may also explain the N(C) observations in diffuse clouds by suitable choices of the density. Similarly, hydrostatic models may also be able to explain observed N(C) in dense clouds (de Jong, Dalgarno, and Boland 1980). But these models must invoke one set of parameters for diffuse clouds and another set of parameters for dense clouds. In contrast, the present model has the attractive potential for explaining both diffuse and dense cloud observations with the same set of relatively simple initial conditions.

A considerably more extensive data base is available for the ubiquitous CO molecules. Figure 8 compares these data with our theoretical results in the form of log N(CO)–log A_v plots. The present theory again agrees with the observations in clouds with $A_v \gtrsim 1$. As is the case for N(C), equilibrium models of interstellar chemistry are also capable of explaining the variation of N(CO) with A_v. The present model, however, goes one step further; it shows (1) that a given cloud may trace the entire observed N(CO)–A_v relation in the source of its dynamical evolution from initial diffuse to final dense state and (2) that the spread in the observed variations of N(CO) with A_v may be attributable to differences in the mass of the clouds. We recognize that N(CO) data for low A_v (<0.6) do not agree with the expectations from the present theoretical curve. One possible explanation is that the N(CO) data for low A_v (<0.6) shown in Figure 8 may be of circumstellar, rather than interstellar, origin. This conjecture is consistent with the findings of Federman *et al.* (1980) that not all interstellar clouds with $A_v \leq 0.6$ show observable CO. Another possibility, suggested by an anonymous referee, is that this disagreement may be due to the neglect of the self-shielding effects in CO photodissociation.

Visual extinction, A_v, loses its significance as an independent parameter after a diffuse cloud has contracted into a dark cloud with $A_v \approx 5$, simply because clouds with $A_v > 5$ are not amenable to precise measurement of this parameter. Core density then becomes a tracer of the evolutionary stage. Our theoretical results for CO in dense phases of evolving clouds are, therefore, shown in the form of f_{CO}–log $n(H_2)$ plots in Figure 9. Theoretical f_{CO} and log $n(H_2)$ in Figure 9 refer to the core where $n(H_2)$ becomes almost uniform. This type of plot is possible because a given cloud spans a large range of core densities (10^4–10^6 cm^{-3}) as it evolves under gravitational contraction. The observational data relate fractional column abundances and the average $n(H_2)$ over the observed CO column as determined by standard density probes, such as H_2CO. The observed decrease in f_{CO} with increasing $n(H_2)$ (Wootten *et al.* 1978) is in agreement with the theoretically predicted decrease solely because of the assumed condensation of CO onto the grains with a sticking probability $s = 0.5$. Equilibrium models cannot account for the decrease of CO with density, because with any reasonable sticking probability CO would be completely removed from the gas phase. In contrast,

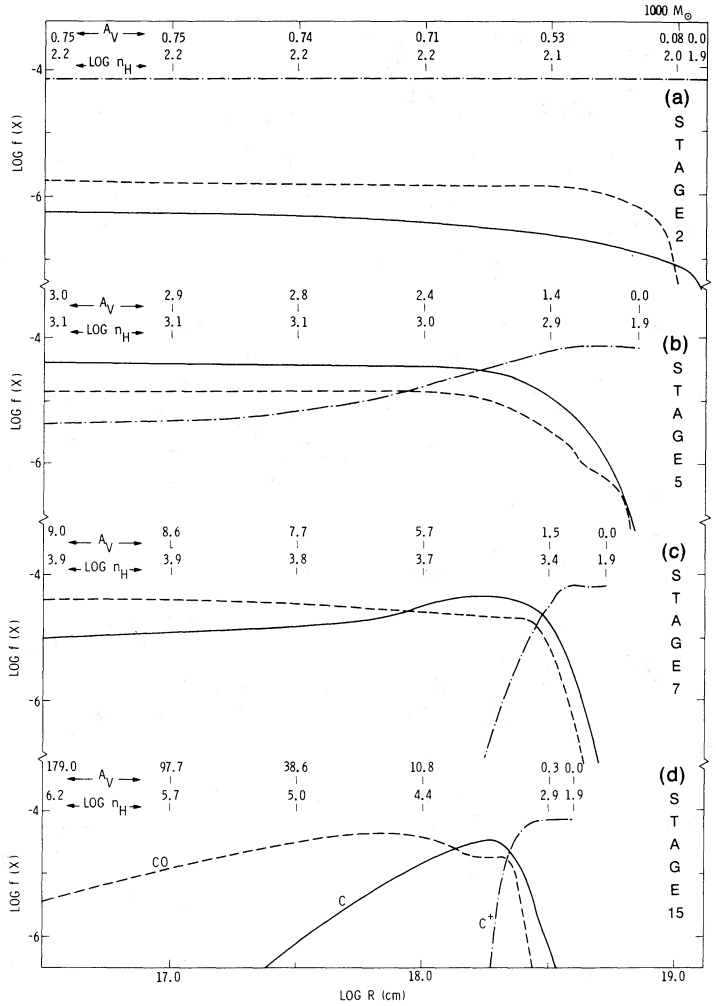

FIG. 6.—Same as Fig. 5, except that the cloud has a mass of 1000 $M_\odot$ and an initial density of 74 cm^{-3}

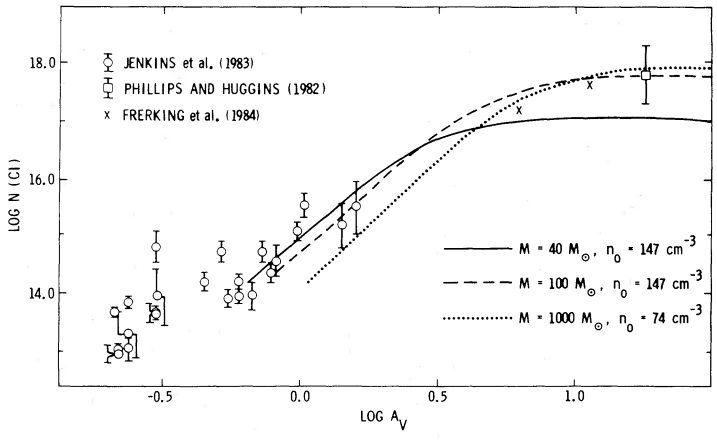

FIG. 7.—Comparison of theoretical and observed variations of N(C I) with A_v

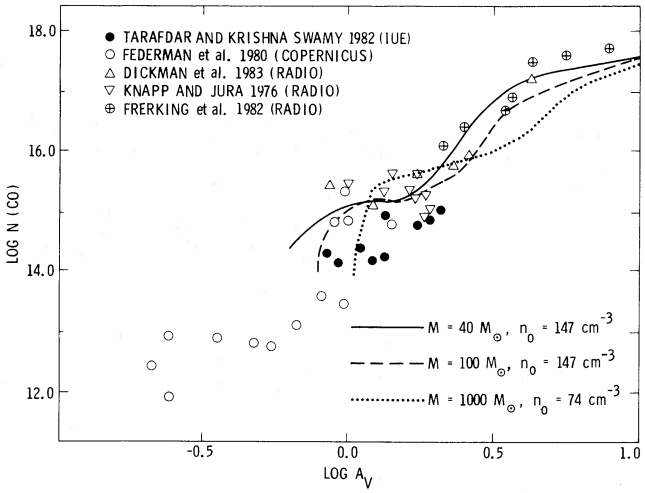

FIG. 8.—Comparison of theoretical and observed variations of N(CO) with A_v.

the present model with s as large as 0.5 is capable of reproducing the observed decrease, because in dynamically evolving clouds a given core density persists for only a limited time and because this time decreases as the density increases. The point is that the condensation onto the grains could not completely deplete CO out of the gas phase within the limited or short lifetime of any given (high) density stage of a dynamically evolving cloud. An alternative way to explain the decrease of CO with increasing core density of clouds without completely eliminating this species from the gas phase is to introduce convective flow in equilibrium models (Boland and de Jong 1982) in an ad hoc manner that may vary from cloud to cloud. In comparison, the present model has the attractive feature that all details follow from first principles and a few simple initial conditions.

Problems associated with line saturation effects complicate the abundance determinations of relatively more abundant species such as CO. Consequently, very recently some doubt has been cast on the reported steep decrease of f_{CO} with n_H, and it is now felt that this decrease may not be as large as those reported in the published literature (N. J. Evans 1984, private communication; W. M. Irvine 1984, private communication). If confirmed, the smaller decrease of f_{CO} with n_H will imply that a smaller effective sticking coefficient should have been used in the present model. The magnitude of the decrease of f_{CO} with n_H predicted by the present dynamical model with $s = 0.5$ is, therefore, not the main issue. They key point is that, compared with static equilibrium models, the present dynamically evolving models are more tolerant of the depletion of molecules onto the grain—in the sense that molecules (CO, for example) have not been wiped out of the gas phase even with $s = 0.5$. In static equilibrium models, sticking of molecules onto the grain would severely deplete gas-phase molecules (see, e.g., Iglesias 1977) unless one assumed either very effective *in situ* desorption mechanisms or circulation currents capable of bringing grains from the inner core to the outer edge at time intervals of the order of 10^6 yr (Boland and de Jong 1982). In the present dynamically evolving models the need for desorption mechanisms or circulation currents would be reduced if the dense cores of the clouds did not live long (i.e., not much longer than 10^5–10^6 yr) after attaining a density of 10^6 cm^{-3}.

A feature of the present theory is that low-mass clouds (40–100 $M_\odot$) appears to be favored over massive clouds (1000 $M_\odot$) by both C and CO observations (see Figs. 7, 8, and 9). This suggests that, beyond $A_v \sim 6$–8, massive clouds may not continue in a state of systematic collapse too long. One possibility is that, at this stage of contraction, the massive clouds fragment as the result of either rotation (Bodenheimer and Black 1978) or thermal-chemical instability (Glassgold and Langer 1976; Sabano and Kannari 1978; Kannari, Sabano, and Tosa 1979).

Our theoretical results for OH and H_2O are presented in Figures 10 and 11, as plots of fractional abundances (f_{OH}, f_{H_2O}) against the radial distance from the center at various stages of evolution. Double peaks with a deep valley between them appear quite spectacular. This feature appears at advanced stages of evolution when the clouds develop a cold, dense core (compare Fig. 10 with Figs. 2, 5, and 6). From numerous previous studies of interstellar chemistry (see § I for an illustrative reference list), it is now well known that concentrations of OH and H_2O in dark, cold regions are controlled by their production from the reaction chain

$$\begin{array}{l} H_2 \xrightarrow{CR} H_2^+ \xrightarrow{H_2} H_3^+ \xrightarrow{O} OH^+ \xrightarrow{H_2} H_2O^+ \xrightarrow{H_2} H_3O^+ \\ \qquad\qquad\qquad\qquad\qquad\qquad\qquad\qquad\quad \downarrow e \qquad\quad \downarrow e \\ \qquad\qquad\qquad\qquad\qquad\qquad\qquad\qquad\quad OH \qquad\quad H_2O \end{array} \tag{13}$$

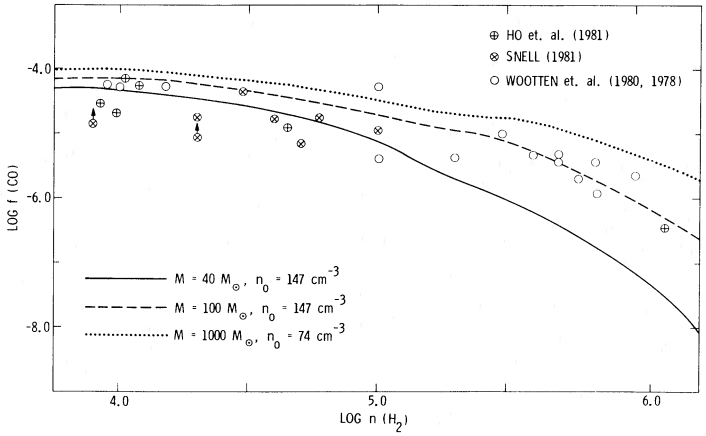

FIG. 9.—Comparison of theoretical and observed variations of fractional abundances f_{CO} with molecular hydrogen density $n(H_2)$. Recently the observed steep decrease of molecular abundances with n_H has become doubtful. This new development and its significance are discussed in the text.

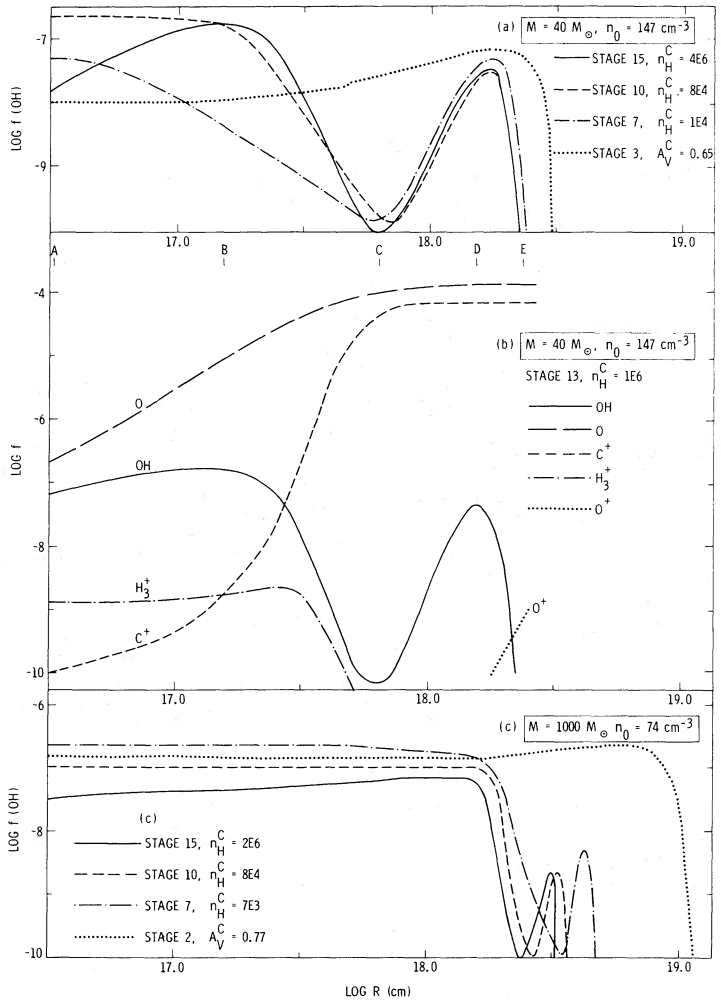

FIG. 10.—Distribution of the fractional abundance f_{OH} at various stages of evolution of (*a*) a 40 $M_\odot$ and (*c*) a 1000 $M_\odot$ cloud. The stages of evolution are specified by either the central density (n_H^c) or the visual extinction (A_v^c). (*b*) Distribution of OH, O, C^+, H_3^+, and O^+ at a stage where $n_H^c = 10^6$ cm^{-3} for a 40 $M_\odot$ cloud; panel *b* is intended to explain the OH distribution as discussed in the text (4E6 ≡ 4 × 10^6, and so on).

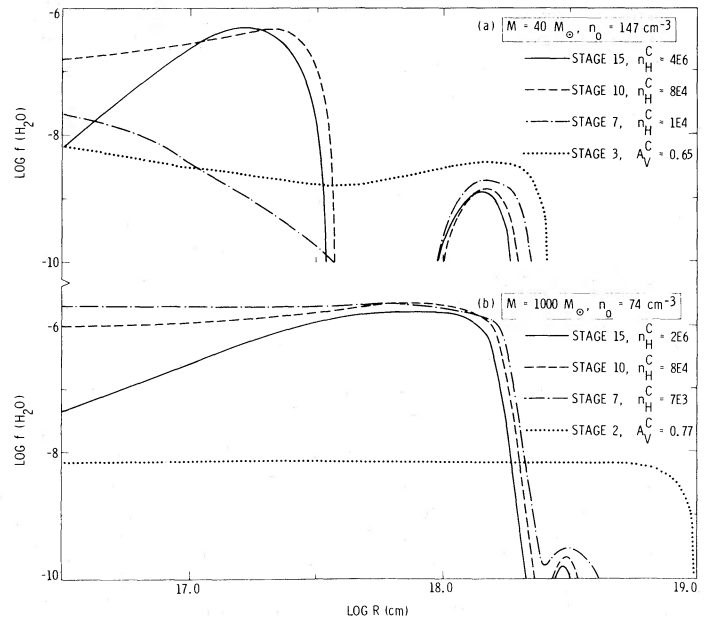

FIG. 11.—Distribution of the fractional abundance f_{H_2O}, at various stages of evolution of (*a*) a 40 $M_\odot$ and (*b*) a 1000 $M_\odot$ cloud. The stages of evolution are specified by either central density (n_H^c) or the visual extinction (A_v).

and by destruction via reactions with O and C^+ and by condensation onto grains, i.e.,

$$OH + O \rightarrow O_2 + H \quad (14a)$$

$$+ C^+ \rightarrow CO^+ + H \quad (14b)$$

$$+ \text{grain} \rightarrow \text{grain} \cdot OH\,, \quad (14c)$$

and

$$H_2O + C^+ \rightarrow HCO^+ + H$$

$$+ \text{grain} \rightarrow \text{grain} \cdot H_2O\,.$$

In hotter regions ($T \geq 60$ K) charge transfer reactions of H^+ with O may become a significant additional source of OH and H_2O via the reaction chain

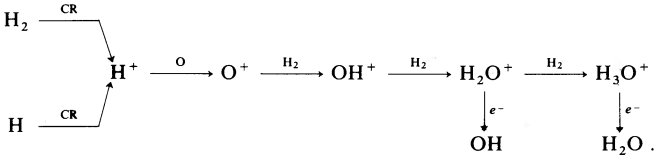

Higher temperatures are needed to activate this channel because the charge transfer reaction $H^+ + O \rightarrow H + O^+$ has an activation temperature 237 K. The importance of this channel, relative to the H_3^+ channel, is also quite dependent upon the $n(H_2)/n_H$ ratio; it is only 5% at the maximum (assuming sufficiently high temperature) when the ratio is 0.5 and approaches 100% as the ratio approaches zero. Furthermore, in the hot regions photodissociation could become the dominant means of destruction of both OH and H_2O because hotter regions of interstellar clouds are generally associated with low A_v (see temperature formulas [10] and [11]).

Given these basic features of interstellar OH chemistry, it is easy to see that the outer and inner peaks in OH distributions are due respectively to O^+ and H_3^+ chemistry. This inference and other details of OH distributions are understandable in light of the data presented in Figure 10*b*. The variation of OH fractional abundance from *A* to *B* follows the variation $f_{H_3^+}$ and f_O in the same region. The decrease of f_{OH} from *B* to *C* is due to decreasing H_3^+ and increasing C^+. The subsequent rise in f_{OH} is due to the rise in the temperature which activates the O^+ channel and the decrease in f_{OH} from *D* to *E* is clearly due to the increased photodissociation. Finally, the low values of f_{OH} at the center of the cloud at evolutionary stage 15 (see Fig. 10*a*) are attributable to condensation onto the grains.

Clearly, the width of the outer peak of OH is determined by the surface temperature T_S and $\partial T/\partial A_v$. On the other hand, the magnitude of the peak would be controlled by the $n_H/n(H_2)$ ratio. In the present work the outer peak is prominent because the surface temperatures of our model clouds are higher and because our $n(H_2)/n_H$ ratios in the $H \rightarrow H_2$ transition zone are also smaller, both relative to their values obtained from first principles using currently known atomic and molecular constants. The higher values result from the use of the semiempirically determined temperature formula and H_2 photodissociation rates as discussed in §§ II*a* and II*b*. Other published theoretical models of dense cloud chemistry (Gerola and Glassgold 1978; de Jong, Dalgarno, and Boland 1980) that attempt to take into account spatial variation of temperature and hydrogen density in dense clouds do not show the outer peak in OH fractional abundance. This may be attributable to those authors' determinations of the temperature distribution and $H \rightarrow H_2$ transition strictly from current theoretical ideas, even though this approach yielded an unrealistically low surface temperature of 42 K at $A_v = 0$ and $n_H = 142$ cm^{-3} (see Table 3 of de Jong, Dalgarno, and Boland 1980). Use of hydrostatic balance, which leads to a steep sech^2 density distribution in the envelope, may also have contributed to the absence of the outer peak in de Jong, Dalgarno, and Boland's (1980) hydrostatic model. Unfortunately, those interesting fine distinctions between the present model and previous equilibrium or dynamically evolving models of dense clouds cannot be verified observationally, because the current techniques of observing OH cannot resolve the outer peak. Nevertheless, the above discussion of the new feature in OH distribution is quite instructive inasmuch as it suggests that the OH distribution in dense clouds may be affected by the cloud's outer environment, such as the external radiation field intensity or proximity of an ultraviolet star. These environmental situations would have the same effect on the temperature distribution and $H \rightarrow H_2$ transition region as our semiempirical modifications of the theory had. Thus, depending upon how close a perturbing ultraviolet star is to a dense cloud, this signature in OH distribution may possibly be observable.

On the basis of the similarities between OH and H_2O chemistries, the outer peaks in the H_2O distributions (Fig. 11) are also due to O^+ chemistry. The outer peaks of f_{H_2O} are, however, considerably less pronounced compared with the outer peaks in f_{OH}. This is partly due to the fact that the outer peak in f_{OH} is strengthened at the expense of that in f_{H_2O}, because photodissociation of H_2O is a source of OH. Furthermore, the inner peak in f_{H_2O} is more pronounced than the inner peak in f_{OH} because chemical destruction of H_2O via reactions with minor ions (e.g., C^+) is relatively very slow. Unfortunately there is a lack of observational data to test our theoretical predictions of f_{H_2O} and its spatial distribution. Observation of H_2O in Orion at 183 GHz (Waters *et al.* 1980) is the only relevant observation. Even so, it is not possible to determine the contributions of "plateau" region and of the extended background cloud. A map of H_2O emission at 380 GHz from Orion using the KAO facility might throw some light on our theoretical results (T. B. H. Kuiper 1983, private communication).

Spatial distributions of CN and HCN at the various stages of evolution of our model clouds are presented in Figure 12. Compared with CN, HCN resides deeper in the core. Hence, HCN could be used as a tracer of the core density of the cloud. Previously the use of HCN as a tracer of density was proposed because excitation of HCN requires high H_2 density. The present calculations clearly add a new justification for using HCN as a tracer of high density, namely, that HCN can be expected to be present only in the dense core of the clouds. Ammonia (NH_3), formaldehyde (H_2CO), and HCO^+ show similar properties. In fact, H_2CO has already been heavily used for density measurements in dense clouds (see, e.g., Snell 1981; Guelin, Langer, and Wilson 1982; Loren, Sandqvist, and Wootten 1983). The HCO^+ ion has also received considerable attention in connection with estimates of electron density in dense clouds (e.g., Wootten, Loren, and Snell 1982; Wootten, Snell, and Glassgold 1979). As a result there is a considerable amount of observational data for HCN, H_2CO, HCO^+, and CN in dense clouds.

Observations of H_2CO, HCN, and CN in dense clouds are compared in Figures 13–15 with the predictions of the present theory. The curves present the theoretical fractional abundance at the center of the cloud as a function of the central $n(H_2)$

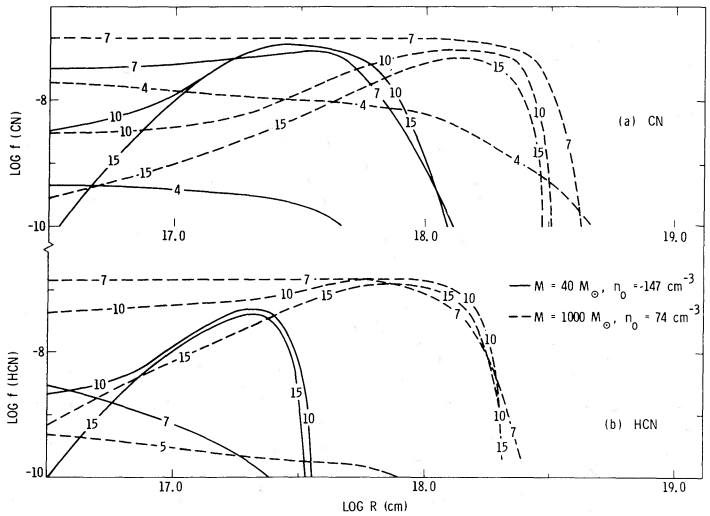

FIG. 12.—Distribution of the fractional abundances (*a*) f_{CN} and (*b*) f_{HCN} at different stages of evolution for clouds of 40 $M_\odot$ (*solid lines*) and 1000 $M_\odot$ (*dashed lines*). The various numerals on the curves represent the progress of evolution in time.

density. The observed quantities are the fractional column abundances and the average density over the observed column. Note that the theoretical and the observed quantities are not exactly the same. In the absence of any knowledge about the spatial extent of the region contributing to the observed column density, it is not possible to construct the exact theoretical counterpart of the observed quantity. The approach used in constructing Figures 13–15 is based on the hope that the central density may be used as a "proxy" for the observed densities. Figures 13–14 show agreement between observation and model values of a 40 $M_\odot$ cloud for H_2CO and HCN, except at low densities, where the theoretical value for HCN is larger than the observed value. The model values for CN, however, are about an order of magnitude larger than its observed values (Fig. 15). Note that Prasad and Huntress (1980*b*) found the theoretical equilibrium values of CN to be about 2 orders of magnitude smaller than the observation in dark clouds. The present overabundance results in spite of the reduction of rate constants of two relevant reactions by a factor of 2 (see reactions 20 and 21 of Table 3 and discussion in Prasad and Huntress 1980*b*). It is not clear at present whether the cause of this discrepancy lies in the uncertainty of rate constants or in the omission of turbulence and rotation in the model, the introduction of which will increase the lifetime of the cloud, decreasing the CN abundance. Even though the theoretical abundances differ from cloud to cloud, the trend with n_H is the same for all clouds. Also, theoretically predicted variation of f_X with n_H is in agreement with the observed variations. This is, of course, a result of including depletion of gas-phase molecules by condensation onto the grains in our chemical reaction network. Considering the various uncertainties involved in treating the condensation of molecules onto the grains (e.g., grain temperature, sticking coefficient), we used a very simplified model with a universal effective sticking

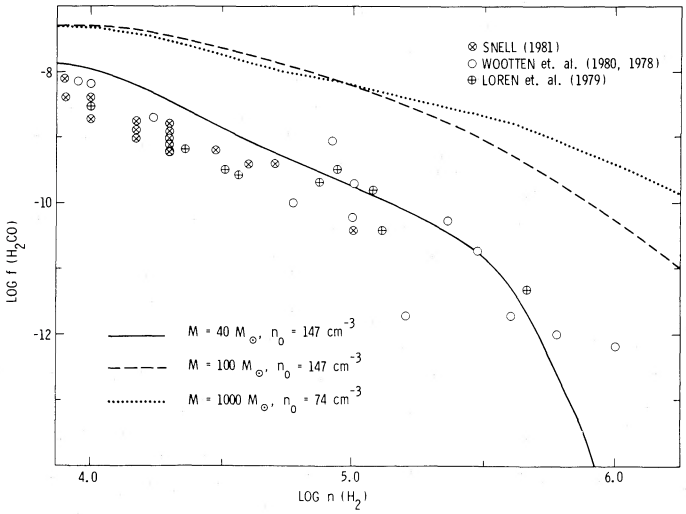

FIG. 13.—Comparison of theoretical and observed variations of the fractional abundance f_{H_2CO} with molecular hydrogen density $n(H_2)$. Recently the observed steep decrease of molecular abundances with n_H has become doubtful. This new development and its significance are discussed in the text.

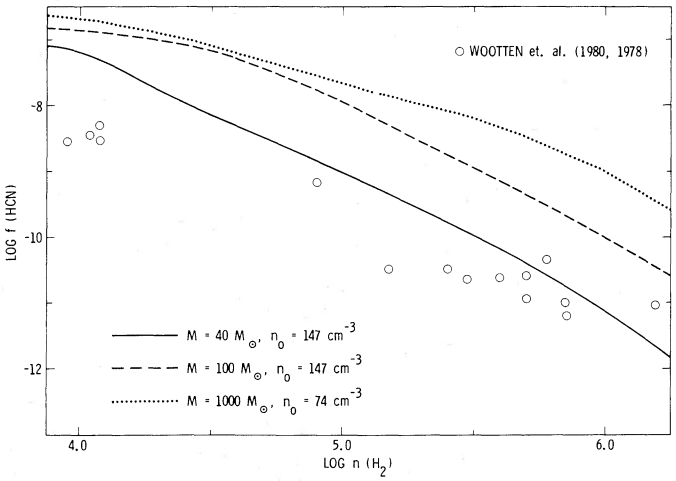

FIG. 14.—Comparison of theoretical and observed variations of the fractional abundance f_{HCN} with molecular hydrogen density $n(H_2)$. Recently the observed steep decrease of molecular abundances with n_H has become doubtful. This new development and its significance are discussed in the text.

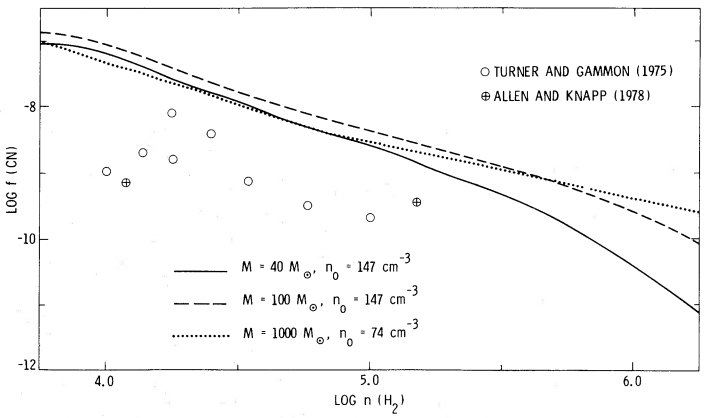

FIG. 15.—Comparison of theoretical and observed variations of the fractional abundance f_{CN} with molecular hydrogen density $n(H_2)$. Recently the observed steep decrease of molecular abundances with n_H has become doubtful. This new development and its significance are discussed in the text.

coefficient of 0.5. Even so, the trend of the theoretical results agrees with observations. It therefore appears possible that condensation onto the grains may be a simple explanation for the observed decrease of molecular abundances with n_H (Wootten, Snell, and Glassgold 1979), provided that the clouds do not live long after attaining a core density of about 10^6 cm^{-3}. Although lifetimes of clouds are uncertain, the possibility exists that molecular clouds are quite transient features and are either dispersed or thoroughly restructured in about 10^7 yr (Larson 1981). As pointed out earlier in connection with the discussion of CO abundance, very recently the large decrease of the fractional abundances of molecules (such as H_2CO) with n_H has become doubtful (N. J. Evans 1984, private communication; W. M. Irvine 1984, private communication). If the actual decrease of f_X (X = H_2CO, HCN, etc.) with n_H is ultimately found to be smaller than those reported in the current literature, then an effective sticking coefficient less than 0.5 would be indicated. This would imply the existence of mechanisms which efficiently counteract the depletion of molecules onto the grains.

Theoretical results for the 40 $M_\odot$ cloud are in better agreement with observations than are the results for the heavier (1000 $M_\odot$) cloud. A similar situation was also encountered in the case of CO. It is difficult to understand this. Furthermore, theoretical results, even for 40 $M_\odot$ clouds, systematically overpredict the abundances. The fact that the reaction network used in the present study was previously fine-tuned with respect to equilibrium models (Prasad and Huntress 1980*a*, *b*) may have contributed to this deficiency of the present model. Furthermore, we had also neglected the existence of chemically significant levels of ultraviolet fluxes in the core of dense clouds due to cosmic-ray excitation of H_2 Lyman and Werner bands as discussed by Prasad and Tarafdar (1983). Inclusion of these ultraviolet photons in the present theory will decrease the theoretical molecular abundances and will thereby lead to improved agreement between the present theory and observations. We are planning to address these issues in the near future.

Finally, Table 4 presents the observed N(H I) and $N(H_2)$ column densities due to atomic and molecular hydrogen in the CO part of a number of clouds from Snell (1981). For comparison, theoretical results are shown in the table. The theoretical results are for a 40 $M_\odot$ cloud when they attain a central or core densities of 1.0×10^4 and 4.1×10^4 cm^{-3}. These central densities bracket the central densities of most of the observed clouds. Theoretical values $5.0 \times 10^{17} \leq N(\text{H I}) \leq 2.6 \times 10^{20}$ cm^{-2} corresponding to $5.4 \times 10^{21} \leq N(H_2) \leq 3.0 \times 10^{22}$ cm^{-2} are consistent with the observed $3.3 \times 10^{18} \leq N(\text{H I}) \leq 8.2 \times 10^{19}$ cm^{-2} corresponding to $1.7 \times 10^{21} \leq N(H_2) \leq 4.4 \times 10^{21}$ cm^{-2}, considering, of course, the uncertainties involved in both theory and observations. Theoretical results in Table 4 also include the total N(H I) and $N(H_2)$. While total $N(H_2)$ is only $\lesssim 2$ times the $N(H_2)$ from the CO region, the total N(H I) is about 2 orders of magnitude larger than N(H I) from the CO region. Thus, the present theory suggests that a CO cloud is always surrounded by a vast H I cloud. This theoretical result agrees with observational findings of Federman and Willson (1982) and Wannier, Lichten, and Morris (1983).

V. SUMMARY AND CONCLUSION

1. We have presented a unified treatment of the dynamical and chemical evolution of initially diffuse, quiescent interstellar clouds of both low and high masses. This treatment naturally accounts for the collapse of low-mass diffuse clouds without requiring them to have initially either unrealistically low temperature, or instabilities or external triggers. This is significant because all previous attempts to collapse low-mass diffuse clouds required these clouds to be either unrealistically cold or subject to instabilities or external triggers such as compression by shocks. Our success has been due to the use of temperatures that depend on both the density and the visual extinction. The dependence of the temperature on the visual extinction generates an inward pressure gradient force that assists gravity in producing the collapse.

2. There is an agreement between the observed and the theoretically predicted A_v dependences of the column densities of various species, such as C and CO, for which a sufficiently large data base is available.

3. In the dense phase of our hydrodynamically evolving cloud there is also an overall agreement between the observed and the theoretically predicted $n(H_2)$ dependence of the fractional column abundances of various molecules and ions, such as H_2CO, HCN, CN, for which sufficiently extensive data exist. Specific discrepancies between the present theoretical results and observations, such as the predicted CN abundance being significantly larger than observed, may be due to inadequacies of the dynamical model or chemical scheme or both. The observed steep decrease of molecular abundances with increasing n_H has, however, recently become doubtful. If the newer

TABLE 4

COMPARISON OF THE OBSERVED AND THEORETICAL COLUMN DENSITIES OF H AND H_2 IN DARK CLOUDS

Clouds	Density $n(H_2)$ in the Central Core (cm^{-3})	Column Densities Associated with the Molecular Region (cm^{-2})		Total Column Density (core + envelope)	
		N(H)	$N(H_2)$	N(H)	$N(H_2)$
L1407	3.0×10^4	$(3.3–11) \times 10^{18}$	3.1×10^{21}	...	...
L1544	2.0×10^4	$(2.4–8.2) \times 10^{19}$	1.9×10^{21}	...	...
L63	4.0×10^4	$(7.4–27) \times 10^{18}$	1.7×10^{21}	...	...
L1235	5.0×10^4	$(9.9–62) \times 10^{18}$	3.2×10^{21}	...	...
L1253	8.0×10^4	$(1.0–3.2) \times 10^{19}$	1.7×10^{21}	...	...
L1257	2.0×10^4	$(1.7–6.3) \times 10^{19}$	4.4×10^{21}	...	...
G_8	1.0×10^4	2.8×10^{18}	5.4×10^{21}	9.4×10^{20}	9.0×10^{21}
G_{10}	4.1×10^4	5.0×10^{17}	1.3×10^{22}	9.3×10^{20}	2.1×10^{22}
A_{10}	1.0×10^4	2.6×10^{20}	1.4×10^{22}	3.3×10^{21}	2.3×10^{22}
A_{12}	4.2×10^4	1.6×10^{19}	3.0×10^{22}	2.2×10^{21}	5.0×10^{22}

NOTE.—Observational data for the various clouds in the Lynds catalog are from Snell 1981. Data for the theoretical model clouds are from the present study. The physical properties of clouds A and G are given in Table 2. Subscripts attached to A and G denote the sequential stages in the collapse. These stages are characterized by the central densities given in the table.

finding that molecular abundances decrease less steeply with n_H is ultimately upheld, then it would imply the existence of mechanisms that efficiently counteract the depletion of molecules onto the grains.

4. The present theory has the potential to explain a wide spectrum of chemical and physical properties of both diffuse and dense clouds with a common formalism employing only a few simple initial conditions. In contrast, previous studies of interstellar chemistry sought to explain diffuse and dark cloud observations using models that may vary from cloud to cloud.

5. The present study suggests the possibility of a unifying link, through hydrodynamic collapse, underlying the great diversity exhibited by interstellar clouds. We may think of families of interstellar clouds, particularly quiescent clouds without any embedded or stellar objects. A given family of such clouds may consist of both diffuse and dark clouds at different stages of evolution. A given family may differ from another with respect to only simple conditions such as cloud mass and initial density.

We emphasize that much more study remains to be done. For example, we must find physical justification for our semi-empirical temperature formula. As a second example, the chemistry of CO, the second most abundant molecule after H_2, should be treated in a more refined manner by including its dissociation by line radiation of the interstellar radiation field and by the ultraviolet radiation field maintained deep inside dense clouds by cosmic-ray excitation of H_2. As a third example, it is necessary to verify the capability of the present model to produce more complex molecules, particularly the long carbon chain molecules, which require many more chemical steps in their synthesis. Also, our theoretical models apply rigorously only to those clouds that do not have embedded protostellar or stellar objects of their own creation.

We thank Peter Bodenheimer for the use of his numerical hydrodynamic code, A. Hindmarsh for the use of his stiff differential equation solver, LSODE, and A. E. Glassgold and W. D. Langer for some constructive comments. Part of the research reported in this paper was performed at the Jet Propulsion Laboratory, California Institute of Technology, under contract with the National Aeronautics and Space Administration.

REFERENCES

Adams, N. G., and Smith, D. 1981, *Chem. Phys. Letters*, **79**, 563.
Allen, M., and Knapp, G. R. 1978, *Ap. J.*, **225**, 863.
Baker, P. L., and Burton, W. B. 1975, *Ap. J.*, **198**, 281.
Bally, J., and Langer, W. D. 1982, *Ap. J.*, **225**, 143.
Barlow, S. E., Dunn, G. H., and Schauer, M. 1984, *Phys. Rev. Letters*, **50**, 902.
Bates, D. R. 1980, *J. Chem. Phys.*, **73**, 1000.
———. 1983, *Ap. J.*, **270**, 564.
Black, J. H., and Dalgarno, A. 1977, *Ap. J. Suppl.*, **34**, 405.
Bodenheimer, P. 1968, *Ap. J.*, **153**, 683.
Bodenheimer, P., and Black, D. C. 1978, in *Protostars and Planets*, ed. T. Gehrels (Tucson: University of Arizona Press), p. 313.
Bodenheimer, P., and Sweigert, A. 1968, *Ap. J.*, **152**, 515.
Bohlin, R. C., Savage, B. D., and Drake, J. F. 1978, *Ap. J.*, **224**, 132.
Boland, W., and deJong, T. 1982, *Ap. J.*, **261**, 110.
de Jong, T., Dalgarno, A., and Boland, W. 1980, *Astr. Ap.*, **91**, 68.
Dickman, R. L., Somerville, W. B., Whittet, D. C. B., McNally, D., and Blades, J. C. 1983, *Ap. J. Suppl.*, **53**, 55.
Federman, S. R., Glassgold, A. E., Jenkins, E. B., and Shaya, E. J. 1980, *Ap. J.*, **242**, 545.
Federman, S. R., Glassgold, A. E., and Kwan, J. 1979, *Ap. J.*, **227**, 446.
Federman, S. R., and Willson, R. F. 1982, *Ap. J.*, **260**, 124.
Field, G. B., 1978, in *Protostars and Planets*, ed. T. Gehrels (Tucson: University of Arizona Press), p. 243.
Frerking, M., Beichman, C. A., Blake, G. A., Keene, J., and Phillips, T. G. 1984, in preparation.
Frerking, M. A., Langer, W. D., and Wilson, R. W. 1982, *Ap. J.*, **262**, 590.
Gerola, H., and Glassgold, A. E. 1978, *Ap. J. Suppl.*, **37**, 1.
Giguere, P. T., and Huebner, W. F. 1978, *Ap. J.*, **223**, 638.
Glassgold, A. E., and Langer, W. D. 1974, *Ap. J.*, **193**, 71.
———. 1976, *Ap. J.*, **206**, 85.
Graedel, T. E., Langer, W. D., and Frerking, M. A. 1982, *Ap. J. Suppl.*, **48**, 321.
Guelin, M., Langer, W. D., and Wilson, R. W. 1982, *Astr. Ap.*, **107**, 107.
Hayashi, C. 1966, *Ann. Rev. Astr. Ap.*, **4**, 171.
Herbst, E. 1976, *Ap. J.*, **205**, 94.
———. 1980*a*, *Ap. J.*, **237**, 462.
———. 1980*b*, *Ap. J.*, **241**, 197.
———. 1983, *Ap. J. Suppl.*, **53**, 41.
Herbst, E., and Klemperer, W. 1973, *Ap. J.*, **185**, 505.
Ho, P. T. P., Martin, R. N., and Barrett, A. H. 1981, *Ap. J.*, **246**, 761.
Huntress, W. T., Jr., McEwan, M. J., Karpas, Z., and Anicich, V. G. 1980, *Ap. J. Suppl.*, **44**, 481.
Iglesias, E. 1977, *Ap. J.*, **218**, 697.
Irvine, W. M., Höglund, B., Friberg, P., Askne, J., and Elldér, J. 1981, *Ap. J.*, **243**, L113.
Jenkins, E. B., Jura, M., and Loewenstein, M. 1983, *Ap. J.*, **270**, 88.
Jenkins, E. B., and Savage, B. D. 1974, *Ap. J.*, **187**, 243.

Joshi, P. 1978, Ph.D. thesis, Tata Institute of Fundamental Research.
Jura, M. 1975*a*, *Ap. J.*, **197**, 575.
———. 1975*b*, *Ap. J.*, **197**, 581.
Kannari, Y., Sabano, Y., and Tosa, M. 1979, *Pub. Astr. Soc. Japan*, **31**, 395.
Kiguchi, M., Suzuki, H., Sata, K., Miki, S., Tominatsu, A., and Nakagawa, Y. 1974, *Pub. Astr. Soc. Japan*, **26**, 499.
Knapp, G. R., and Jura, M. 1976, *Ap. J.*, **209**, 782.
Larson, R. B. 1973, *Ann. Rev. Astr. Ap.*, **11**, 219.
———. 1981, *M.N.R.A.S.*, **194**, 809.
Lequeux, J. 1977, in *IAU Symposium 75, Star Formation*, ed. T. de Jong and A. Maeder (Dordrecht: Reidel), p. 69.
Loren, R. B., Evans, N. J., II, and Knapp, G. R. 1979, *Ap. J.*, **234**, 932.
Loren, R. B., Sandqvist, A., and Wootten, A. 1983, *Ap. J.*, **270**, 620.
Lynds, B. T. 1962, *Ap. J. Suppl.*, **7**, 1.
McNally, D. 1971, *Rept. Progr. Phys.*, **34**, 71.
Mitchell, G. F., Ginsburg, J. L., and Kuntz, P. J. 1978, *Ap. J. Suppl.*, **38**, 39.
Mitchell, G. F., Prasad, S. S., and Huntress, W. T., Jr. 1981, *Ap. J.*, **244**, 1087.
Oppenheimer, M., and Dalgarno, A. 1975, *Ap. J.*, **200**, 419.
Phillips, T. G., and Huggins, P. J. 1982, *Ap. J.*, **251**, 533.
Phillips, T. G., Huggins, P. J., Kuiper, T. B. H., and Miller, R. E. 1980, *Ap. J. (Letters)*, **238**, L103.
Pickles, J. B., and Williams, D. A. 1977, *Ap. Space Sci.*, **52**, 453.
Prasad, S. S., and Huntress, W. T., Jr. 1980*a*, *Ap. J. Suppl.*, **43**, 1 (PH).
———. 1980*b*, *Ap. J.*, **239**, 151.
Prasad, S. S., and Tarafdar, S. P. 1983, *Ap. J.*, **267**, 603.
Sabano, Y., and Kannari, Y. 1978, *Pub. Astr. Soc. Japan*, **30**, 77.
Savage, B. D., Bohlin, R. C., Drake, J. F., and Budich, W. 1977, *Ap. J.*, **216**, 291.
Scoville, N. Z., and Solomon, P. M. 1975, *Ap. J. (Letters)*, **199**, L105.
Smith, D., and Adams, N. G. 1978, *Ap. J. (Letters)*, **220**, L87.
Smith, L. F., Biermann, P., and Mezger, P. G. 1978, *Astr. Ap.*, **66**, 65.
Snell, R. L. 1981, *Ap. J. Suppl.*, **45**, 121.
Solomon, P. M., and Klemperer, W. 1972, *Ap. J.*, **178**, 389.
Suzuki, H., Miki, S., Sata, K., Kiguchi, M., and Nakagawa, Y. 1976, *Progr. Theoret. Phys. (Japan)*, **56**, 1111.
Tarafdar, S. P., and Krishna Swamy, K. S. 1982, *M.N.R.A.S.*, **200**, 431.
Taylor, R. J. 1968, *Rept. Progr. Phys.*, **31**, 167.
Turner, B. E., and Gammon, R. H. 1975, *Ap. J.*, **198**, 71.
Villere, K. R., and Black, D. C. 1980, *Ap. J.*, **236**, 192.
———. 1982, *Ap. J.*, **252**, 524.
Wannier, P. G., Lichten, S. M., and Morris, M. 1983, *Ap. J.*, **268**, 727.
Waters, J. W., *et al.* 1980, *Ap. J.*, **235**, 57.
Woolfson, M. M. 1979, *Phil. Trans Roy. Soc. London, A*, **291**, 219.
Wootten, A., Bozyan, E. P., Garrett, D. B., Loren, R. B., and Snell, R. L. 1980, *Ap. J.*, **239**, 844.
Wootten, A., Evans, N. J., II, Snell, R., and Vanden Bout, P. 1978, *Ap. J. (Letters)*, **225**, L143.
Wootten, A., Loren, R. B., and Snell, R. L. 1982, *Ap. J.*, **255**, 160.
Wootten, A., Snell, R., and Glassgold, A. E. 1979, *Ap. J.*, **234**, 876.
Zuckerman, B., and Palmer, P. 1974, *Ann. Rev. Astr. Ap.*, **12**, 279.

DAVID C. BLACK and KAREN R. VILLERE: NASA/Ames Research Center, Mail Stop 245-3, Moffett Field, CA 94035

WESLEY T. HUNTRESS, JR.: Jet Propulsion Laboratory, Mail Stop 183-301, 4800 Oak Grove Drive, Pasadena, CA 91109

SHEO S. PRASAD: Jet Propulsion Laboratory, Mail Stop 183-601, 4800 Oak Grove Drive, Pasadena, CA 91109

SHANKAR P. TARAFDAR: Theoretical Astrophysics Branch, Tata Institute of Fundamental Research, Homi J. Bhabha Road, Bombay-400 005, India